coatings

MDPI

Article

Combined Use of Surface Texturing, Plasma Nitriding and DLC Coating on Tool Steel

Elisangela Aparecida dos Santos de Almeida [1], Julio Cesar Giubilei Milan [1], César Edil da Costa [1], Cristiano Binder [2], José Daniel Biasoli de Mello [2,3] and Henara Lillian Costa [4,*]

[1] Department of Mechanical Engineering, Universidade do Estado de Santa Catarina, Joinville 89219-710, Brazil; elisangela_s_almeida@yahoo.com.br (E.A.d.S.d.A.); julio.milan@udesc.br (J.C.G.M.); cesar.edil@udesc.br (C.E.d.C.)
[2] Materials Laboratory (Labmat), Universidade Federal de Santa Catarina, Florianópolis 88040-900, Brazil; cristiano.binder@labmat.ufsc.br (C.B.); ltm-demello@ufu.br (J.D.B.d.M.)
[3] Laboratory of Tribology and Materials, Universidade Federal de Uberlandia, Uberlândia 38408-100, Brazil
[4] School of Engineering, Universidade Federal do Rio Grande, Rio Grande 96203-900, Brazil
* Correspondence: henaracosta@furg.br

Abstract: In cold rolling, a textured roll can be used to imprint a desired surface topography onto the sheet during rolling. This work proposes the use of diamond-like carbon (DLC) coatings to protect the surface topography of the rolls in replacement of the carcinogenic hard chrome. For that, hydrogenated amorphous carbon (a-C:H) was deposited on plasma nitrided tool steel, both for ground and textured specimens. Changes in surface topography due to DLC coating were assessed using a confocal microscope. Coating adhesion was evaluated using the method VDI 3198. The specimens were characterized using X-ray diffraction (XRD), microhardness test and scanning electron microscopy (SEM). The coating was characterized using Raman spectroscopy (RS) and X-ray photoelectron spectroscopy (XPS). The results showed a soft multilayer coating consisting of a plasma nitrided layer for load support, a Si-rich interlayer to improve adhesion and an a-C:H top layer. DLC deposition reduced the roughness of the textured specimens. The coating resulted in relatively stable friction and good durability, with small damage and negligible wear even under dry sliding.

Keywords: DLC; surface texturing; plasma nitriding; cold rolling

Citation: dos Santos de Almeida, E.A.; Milan, J.C.G.; da Costa, C.E.; Binder, C.; de Mello, J.D.B.; Costa, H.L. Combined Use of Surface Texturing, Plasma Nitriding and DLC Coating on Tool Steel. *Coatings* **2021**, *11*, 201. https://doi.org/10.3390/coatings11020201

Academic Editors: Carsten Gachot and Philipp Grützmacher
Received: 3 December 2020
Accepted: 3 February 2021
Published: 9 February 2021

1. Introduction

Metalforming applications involve very high contact pressures, posing tribological challenges to the quality of the final product and the tool life. Advanced approaches for surface engineering can greatly improve tribological properties during metalforming. Among those, surface textures [1–5], plasma nitriding [6–8] and coatings [5,8–11] are promising avenues being explored to improve friction and wear of metalforming tools.

In cold rolling, surface texturing of the roll is a current practice. The roll texture is transferred to the sheet during rolling, improving the aesthetic characteristics of the rolled sheet [12,13]. Moreover, texturing of the roll can improve tribological performance during rolling, either by removing wear debris from the contact [2], by acting as lubricant reservoirs [4] or by generating plastohydrostatic and plastohydrodynamic lubrication mechanisms [14]. Surface textures in cold rolling are commonly random, produced by sandblasting or electric discharge texturing (EDT) [13].

However, the high contact pressures involved in metal forming lead to fast removal of the surface textures by wear. This can be mitigated by the use of hard coatings after surface texturing [15]. Hard chrome coatings have been widely used for this purpose [5], but health issues related to the deposition of hard chrome plating have been restricting its use in industry [16], despite industrial efforts to reduce these problems [17]. Alternative coatings for the replacement of hard chrome have been proposed, such as chromium nitride [18] and

Co-Ni-P coating [19]. Recently, our groups have compared the tribological performance of hard chrome with plasma nitriding and electroless NiP coatings on both textured and untextured tool steel specimens. The tribological behavior of plasma nitriding in terms of the friction, wear and life of the textures was comparable (and sometimes slightly inferior) to that of hard chrome, and substantially worse than that of NiP. The superior performance of NiP in relation to both hard chrome and plasma nitriding was attributed to the formation of a protective tribolayer rich in Ni, P and O on both the specimens and the counterbodies [8].

Another important family of potential coatings for use in cold rolling is diamond-like carbon (DLC), a metastable form of amorphous carbon with a high ratio of tetrahedral sp^3 (diamond) to sp^2 (graphite) bonds, therefore combining characteristics of both diamond and graphite [20,21]. The literature has shown that by changing the sp^3/sp^2 ratios of carbonous materials, diamond, ordered graphite or amorphous graphite can be obtained, tuning their properties accordingly [22]. This unusual combination of properties includes high hardness, low friction coefficient, high corrosion resistance, biocompatibility and hemocompatibility [23], small surface roughness and optical transparency [24], and semiconductivity [21]. Furthermore, thermal and electrical conductivity can be tuned depending on the amount of sp^3 and sp^2 bonds. Some of those properties (high hardness, elastic modulus and chemical inertness) are similar to those of diamond, due to the significant fraction of (sp^3) hybridization, and also due to the fact that a disordered thin film does not present grain boundaries, but DLC films are much cheaper to produce than diamond films [25]. The high stiffness and hardness often result in low friction and wear, due to the reduced contact area.

DLC films can be doped or bonded with nitrogen, silicon and sulfur, among others, leading to superior mechanical, thermal and tribological properties [26]. The incorporation of silicon, for example, promotes friction reduction, increases durability, improves stability in humid environments and temperature, and promotes better surface finish and increased adhesion of the film to the substrate [27].

However, when deposited onto softer substrates, the resulting stress distribution can lead to spalling of the DLC coating. The combination of multilayers (such as CrN + DLC) increases the loading capacity of the substrate, improving adhesion and leading to a more favorable stress distribution [28]. Plasma nitriding of the substrate is another approach to improve load-bearing capacity before DLC deposition [29]. It allows progressively increase surface hardness, creating mechanical support for the DLC coating [30]. The adhesion between the DLC coating and the softer substrate is particularly relevant for a textured surface, since the surface topography affects this adhesion [31]. Moreover, the surface roughness of the substrate has a strong effect on the friction and wear of DLCs [29,31]. The microstructure of the nitrided zone consists of a compound layer (surface layer) and a diffusion zone underneath the compound layer. Depending on the nitrogen concentration in the gas mixture used during plasma nitriding, the compound layer may be constituted by ε-$Fe_{2-3}N$ (hcp arrangement of Fe atoms with ordered occupation of the N atoms at the octahedral interstitial sites) or γ'-Fe_4N (fcc arrangement of Fe atoms with ordered occupation of the N atoms at the octahedral interstitial sites) phases, or a mixture of both [32]. In the diffusion zone, nitrogen is either dissolved interstitially in the octahedral interstitial sites of a bcc ferrite matrix, or precipitated as γ'-Fe_4N and α''-$Fe_{16}N_2$ (bct arrangement of iron atoms with ordered occupation of N at the octahedral interstitial sites) nitrides [33]. Significant changes have been observed in surface topography due to nitriding for compound layers predominantly of γ' phase [27,34]. This occurs because the nitride layer is obtained by accelerating N^+ ions against the substrate, responsible for cleaning, heating and providing active N to diffuse into the material, but at the same time modifying the surface topography of the substrate [30].

Despite the large potential of DLC coatings to control friction and reduce wear, increasing the life of textured tools, the use of DLC on textured tools is particularly challenging. EDT leads to a rough surface, and therefore contact pressures at the asperity level are very

high [15], which can lead to spallation of the DLC coating. Probably for this reason, in a very recent review about the combined use of surface texturing and solid lubricants, where 269 articles were reviewed, no reference was found for the use of DLC to protect textured metal forming tools [35]. With that in mind, the rationale of this work involved using an alternative route for DLC synthesis that could result in soft DLC. Despite the expected lower hardness, a soft DLC could potentially result in reduced spallation, thus withstanding the high contact pressures with adequate tribological performance.

Therefore, this work investigates the combination of plasma nitriding with DLC deposition of a relatively soft amorphous hydrogenated carbon (aC:H) film using a Si-rich DLC interlayer on textured tool steel surface, which is compared with a ground surface. Microhardness measurements, nanoindentation, Raman spectroscopy (RS), confocal microscopy and X-ray photoelectron spectroscopy (XPS) analysis evaluate the coatings produced, and preliminary pin-on-disk tests evaluate their performance under dry and lubricated conditions.

2. Materials and Methods

2.1. Specimen Preparation

Specimens measuring 35 × 35 × 5 mm^3 were used in this work, which were cut from a fragment of an industrial roll used in rolling mills. The material of the roll was a proprietary Gerdau VC10 tool steel, with nominal chemical composition (wt.%) of 0.76–1.05 C, 4.3–4.7 Cr, 0.5–0.8 Mn, 0.1–0.45 Si, 0.11–0.39 Mo. The chemical composition of the specimens, obtained via optical emission spectrometry, is shown in Table 1. According to the manufacturer of the roll, quenching and tempering is used to achieve suitable hardness. The Vickers hardness of the specimens was measured as HV_{10} = 611 ± 30, and the microstructure apparently consisted of martensite (Figure 1). After cutting, they were ground on both faces to ensure their parallelism. They then underwent the following sequence of surface treatment: texturing by EDT, followed by plasma nitriding and finally DLC deposition.

Table 1. Chemical composition of the tool steel specimens.

	C	Cr	Mo	Mn	Si	Ni	P	S	W	V	Fe
Amount (wt.%)	0.86	4.50	0.22	0.60	0.27	0.13	0.012	0.009	0.0007	0.0705	Balance

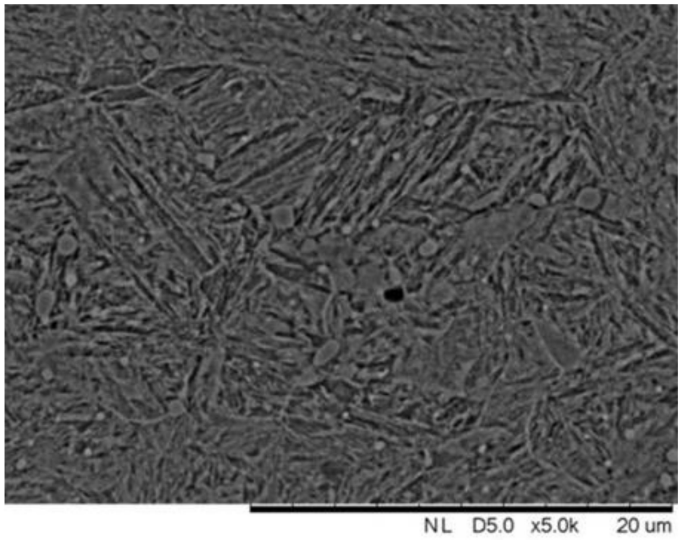

Figure 1. Scanning electron microscopy (SEM) of the specimens before the surface treatments.

Samples were textured using an EDT process, using an equipment model Engemaq 440 MC, electrolytic copper electrodes and a hydrocarbon-based dielectric fluid (Arclean

Eletron). The area textured was 20 × 20 mm^2, the discharge current (pulsed) was 9A, the pulse time was 20 ms and the duty cycle was 16%, given by the pulse time (t_{on}) divided by total time ($t_{on} + t_{off}$).

2.2. Plasma Nitriding and DLC Deposition

A PECVD duplex treatment using an industrial scale reactor was performed consisting of a nitriding step (550 °C, 90 min) followed by a silicon-rich interlayer deposition using hexamethyldisiloxane (HMDS) as precursor (260 °C, 30 min) and an a-C:H layer as the uppermost low friction film (250 °C, 20 min), all steps in the same reactor. The parameters used for the nitriding treatment and film deposition are listed in Table 2, which were selected aiming to produce a soft DLC.

Table 2. Plasma nitriding and diamond-like carbon (DLC) deposition conditions.

Scheme	Temperature (°C)	Time (min)	Bias (V)	Pressure (Torr)	Power (W)	Duty Cycle (%)	Atmosphere
Plasma nitriding	550	90	350	3.0	400	80	9% H_2, 90% N_2 and 1% CH_4
DLC layer 1	260	30	400–500	1.5	90	15	(2–5%) HMDS + (65–68%) CH_4 + 10% Ar + 20% H_2
DLC layer 2	250	25	400–500	1.5	90	10	20% H_2 and 80% CH_4

2.3. Characterization of the Treated Surfaces

The surface roughness of the specimens before texturing, after texturing by EDT and after plasma nitriding + DLC deposition was measured using a confocal microscope model Leica DCM3D. Three areas of 1 mm × 1 mm were measured for each surface condition. The analysis used the software Mountainsmap®. The parameters chosen to quantify the surface topography were: *Sq* (root mean square roughness of the surface, in μm); *Ssk* (skewness, to assess the asymmetry of the height distribution curve); *Sku* (kurtosis, to assess the flattening factor of the height distribution curve); *Sdq* (hybrid parameter representing the mean slope of the irregularities); *Spk* (parameter associated with the Abbott-Firestone curve, representing the height of the peaks that would be removed first during running-in); *Svk* (parameter associated with the Abbott-Firestone curve, representing the valley depths that can be related to oil retention capacity for lubrication); and *Sbi* (representing the mechanical support capacity of the surface). Before calculation of the parameters, a levelling tool was used, but no further filtering to remove waviness was applied.

After deposition, cross-sections were carefully prepared to identify the nitrided layer (diffusion and compound layers) and DLC coating. Before cutting the cross-sections, the specimens were coated by electrodeposition with a thin Ni layer to protect the coating, avoiding spallation during cutting. The polished cross sections were etched with Nital. Vickers microhardness of the specimens was measured using 100 g (HV0,1) for 10 s on the cross-sections both on the substrate and the compound layer, as an average value of five indentations.

To evaluate the mechanical properties of the DLC film, instrumented nanoindentation tests were performed according to Oliver and Pharr methodology [12]. The normal load used was 10 mN and the results of nanohardness and elastic modulus represent an average of 14 measurements. The nanoindentation measurements were only performed for the DLC coating deposited onto the ground specimen, since the very rough textured specimen should result in measurement deviation [13].

The coating adhesion to the surface was evaluated according to the method VDI 3198 [14], where the damage caused by the indentation is compared to a map used to classify the failure modes. For that, the vicinity of the Rockwell C indentation, produced using a universal hardness tester model VEB Werkstorfpruffmaschinen, was assessed by scanning electron microscopy (SEM) using a field emission gun equipment model FEG-JEOL-JSM 6107F.

The crystalline phases present in each specimen were identified by X-ray diffraction (XRD) with Cu-Kα and 2θ radiation ranging from 20–90°. XRD measurements were carried out in a ground specimen after plasma nitriding and DLC deposition. Since the amorphous DLC film does not present crystalline phases, the Bragg–Brentano θ-2θ configuration was used to assess the phases present in the substrate in the steel substrate and nitrided layer. The penetration depth of the X-ray measurements was estimated as 4.51 of 4.66 μm (see Section 3.2). The nature of the DLC chemical bondings was characterized by RS (equipment model Renishaw 2000) with an argon laser and wavelength (λ) of 514.5 nm. The Raman shift was evaluated from 1000 to 1800 cm^{-1}. This range includes DLC characteristic bands corresponding according to the literature to bands D and G, respectively related to disorder and graphite [21]. Two analyses were performed for each surface condition. The hydrogen percentage in the films was obtained from the Raman measurements following the method proposed by Casiraghi et al. [36], and the amount of H was computed according to Equation (1), where m is the slope of the baseline used to obtain the intensities of the bands D and G and I(G) is the intensity of peak G.

$$H[\%at] = 21.7 + 16.6log\left(\frac{m}{I(G)}\right) \quad (1)$$

XPS analysis of the coated specimens was performed in a bench equipment model Thermo Scientific K-Alpha, with base pressure of 10^{-8} mbar and Al-Kα ($h\nu$ = 1486. 6 eV) X-ray source, in order to quantify the DLC film chemical composition. Peak deconvolution was performed using CASAXPS software.

2.4. Tribological Tests

Tribological tests under a limited range of conditions were used for an initial assessment of the friction and wear of the different surface conditions. The aim was not to fully evaluate their tribological performance, but to provide a general view of how the combination of EDT, plasma nitriding and DLC deposition performs under high contact pressure conditions. For that, room temperature ball-on-flat unidirectional tests were carried out under dry and limited lubricant supply conditions (starved lubrication). The conditions for the tribological tests are summarized in Table 3. The lubricant in the lubricated tests was a polyalphaolefin base oil without additives, specification PAO 8, density of 834 kg.m^3, kinematic viscosity at 40 °C of 46.4·10^{-6} $m^2 \cdot s^{-1}$, and viscosity index of 138.

Table 3. Conditions of the tribological tests.

Sliding speed	0.3 $m \cdot s^{-1}$
Track radius	6 mm
Normal load	10 N
Sliding distance	1000 m
Counterbody	AISI 52,100 steel ball, ϕ = 6 mm
Lubrication regimes	Dry and starved lubrication
Lubricant volume	0.7 mL

The calculation of the initial Hertzian pressure at the beginning of the tests (P_{max}, Equation (2)) used the normal load (W) of 10N, E_{steel} = 210 GPa, ν_{steel} = 0.3, radius (R) of the ball = 3 mm. The values of E and ν for the DLC film were measured by nanoindentation (see Results section) as 59.9 GPa and 0.25, respectively.

$$P_{max} = \frac{1}{\pi}\sqrt[3]{\left(\frac{6E^{*2}W}{R'^2}\right)} \quad (2)$$

where E^* is the combined Young´s modulus of the two contacting materials given by $1/E^* = (1 - {\nu_1}^2)/E_1 + (1 - {\nu_2}^2)/E2$, R' is the combined radius given $1/R' = (1)/R_1 + (1)/R_2$, $R_2 = \infty$ (plane). The values of Poisson ratios of the steel ball (ν_1) and of the DLC (ν_2) [37]

were obtained from the literature as 0.33 and 0.3, respectively. This resulted in values of *Pmax* = 1.42 GPa for the uncoated surfaces and 0.81 GPa for the DLC-coated surfaces.

3. Results

3.1. Surface Morphology

The surface morphology of the different specimens is depicted by secondary electron (SE) SEM images in Figure 2. The grinding marks were still visible after DLC deposition in Figure 2b, but the morphology appeared slightly smoothed when compared with the ground condition (Figure 2a). The morphology of the specimen textured by EDT (Figure 2c) shows recessed throughs corresponding to the ablated regions during EDT, as well as protruding features, corresponding to recast material, which is the typical morphology for surfaces textured by EDT [5,13]. For DLC deposition after EDT (Figure 2d), the morphology resembled that for EDT, but the surfaces appeared substantially smoother. In particular, the recessed throughs became less visible, apparently coated with DLC.

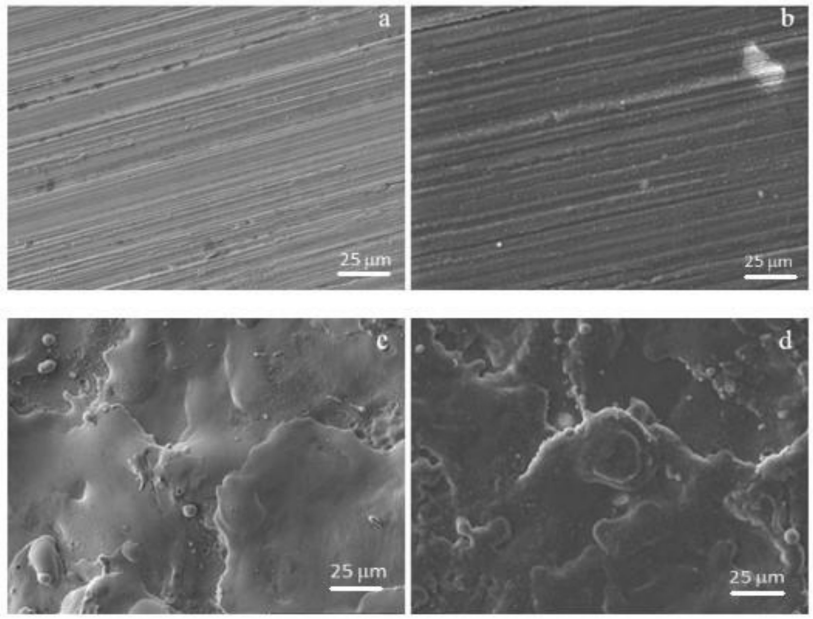

Figure 2. Secondary electron (SE) SEM images of the different surface conditions: (**a**) ground; (**b**) ground + DLC; (**c**) electric discharge texturing (EDT); and (**d**) EDT + DLC.

A cross-section of the coated specimens is exemplified in Figure 3 for the ground condition. The average thickness of the DLC coating was 2.44 ± 0.33 µm (average of 14 measurements). The compound layer (also called white layer) had a thickness of 9.62 ± 0.67 µm, and the diffusion zone measured approximately 80 µm.

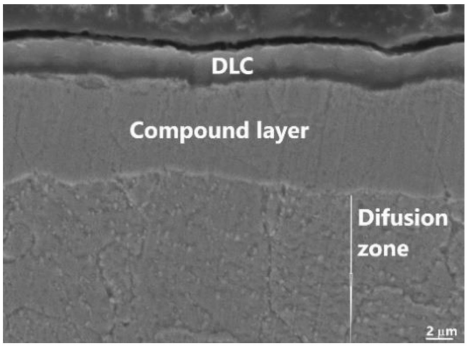

Figure 3. Cross-section of the ground specimen after plasma nitriding and DLC deposition.

In order to quantify how DLC deposition affected the surface topography of the specimens, the height parameters (*Sq, Spk, Svk*) and the hybrid parameter *Sdq* are presented in Figure 4. Since the values measured for the textured specimens were around one order of magnitude higher, the ground specimens are shown in Figure 4a, and the textured specimens in Figure 4b. For the ground specimens, the height parameters *Sq*, *Spk* and *Svk* reduced 20%, 26% and 25%, respectively, after plasma nitriding + DLC deposition. Reduction in a similar range (27%) was observed for the average slope of the asperities (*Sdq*). Although the error bars were large, Anova tests ($\alpha = 0.05$) showed that the differences were statistically significant. As expected, the textured specimens were substantially rougher than the ground specimens. It is worth mentioning the large values of *Svk* before DLC deposition, evidencing large valley depths. When the EDT specimens were plasma nitrided and then coated with DLC, the reduction of the roughness parameters was much higher than for the ground specimens, 54% for *Sq*, 72% for *Spk*, 73% for *Svk* and 86% for *Sdq*.

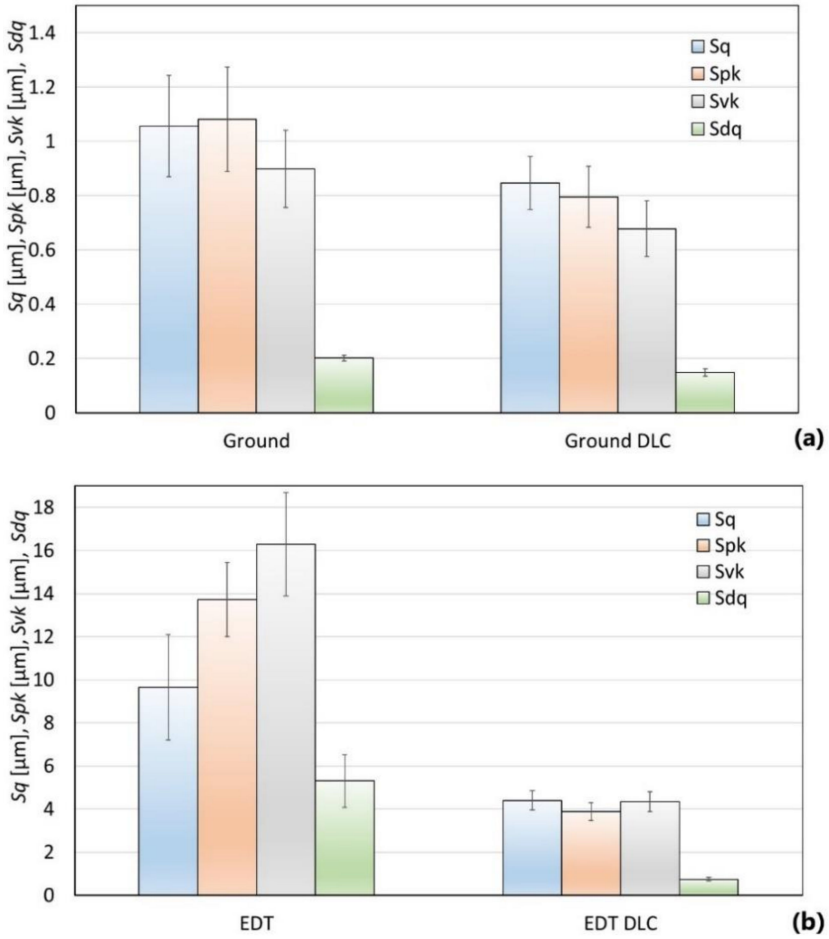

Figure 4. *Sq, Spk, Svk* and *Sdq* values: (**a**) ground condition; (**b**) EDT condition.

Regarding the parameters *Ssk* and *Sku*, the literature suggests that their simultaneous analysis by plotting *Sku* as a function of *Ssk* provides an interesting morphological analysis of the surface [38]. The morphological space S_{ku} versus S_{sk} (Figure 5) enables to identify groups with similar behaviors, as well as morphological changes due to surface treatment. The ground specimens, both uncoated and coated presented *Sku* values close to 3 and *Ssk* values close to 0, were typical of a Gaussian height distribution. This region is encapsulated in red in Figure 5. The textured specimen showed very large *Sku* values and negative values of *Ssk*, appearing in a very distinct region of the morphological space, encapsulated in green. *Sku* is associated with the kurtosis of the curve of height distribution, where *Sku* values larger than 3 indicate a peaked height distribution. *Ssk* is associated with the

symmetry of the height distribution curve, where negative *Ssk* values correspond to a plateau-valley distribution. Since the error bars both for *Sku* and *Ssk* values were very large, the surfaces were highly non-uniform, ranging from predominantly plateau-valley morphologies to a few areas with plateau-peak morphology. When the textured specimen was plasma nitrided and DLC-coated, the *Sku* value approached 3, which was typical of a Gaussian distribution, but with much smaller error bars than the EDT specimen. The curve remained negatively asymmetric (*Ssk* < 0), still indicating preponderance of valleys, but to a smaller extent than the EDT specimen, as well as less scattering (blue capsule).

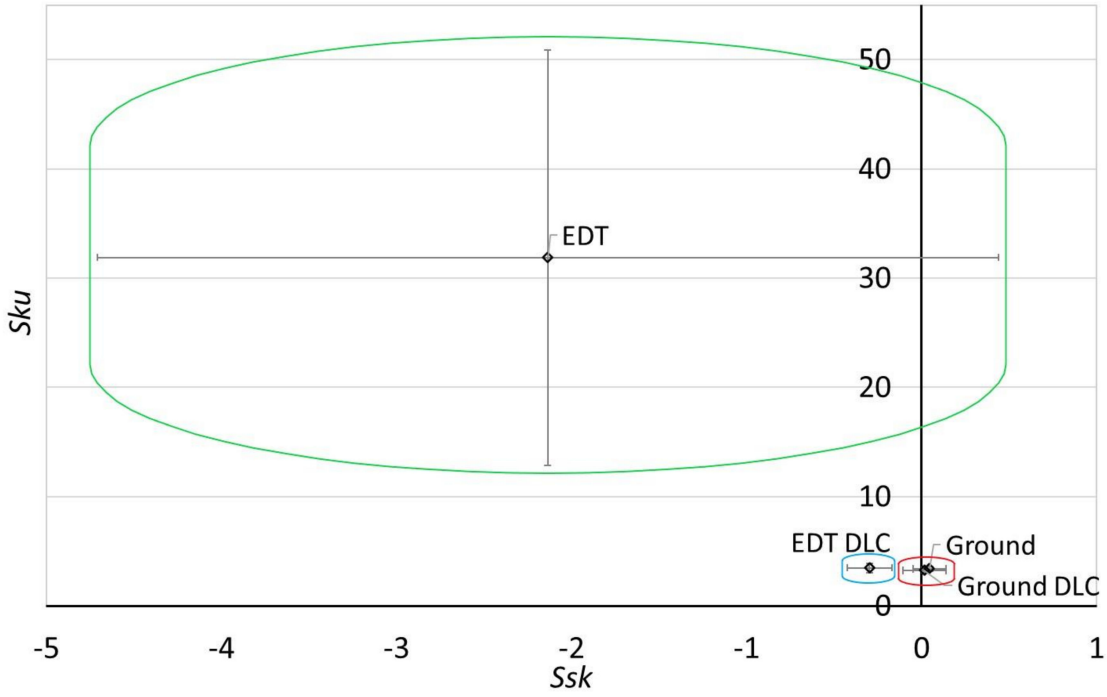

Figure 5. Morphological space *Ssk* versus *Sku*.

Sbi values for all the surface conditions are presented in Figure 6. For the ground specimen, plasma nitriding + DLC did not affect the load-bearing capacity of the surface. The textured specimens showed lower bearing capacity than the ground specimens. After plasma nitriding + DLC, *Sbi* increased; Anova tests showed that statistically, the load-bearing capacity for EDT DLC was not different from either ground or ground DLC.

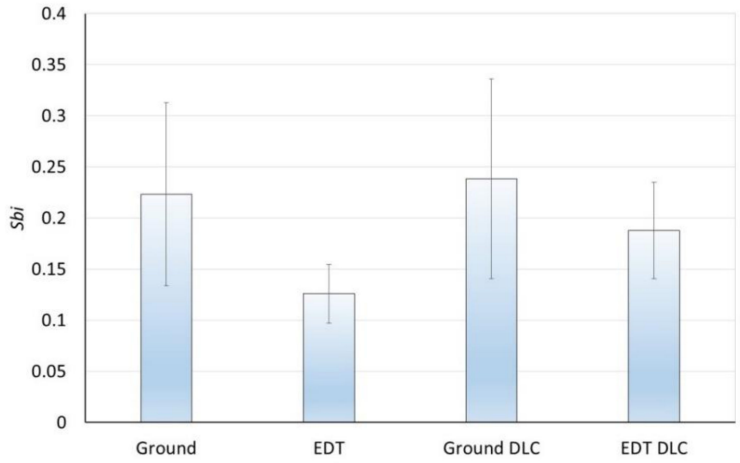

Figure 6. *Sbi* values for the different surface conditions.

3.2. Structure and Mechanical Properties of the Modified Surfaces

XRD diffractograms of the specimens before and after plasma nitriding + DLC deposition are presented in Figure 7. Peak 1 could correspond to ferrite or martensite, but considering the hardness and microstructure of the specimens, it was assigned to martensite. For the specimen with plasma nitriding + DLC, peak 1 was no longer present, while peaks for the $Fe_{2-3}N$ (ε) and Fe_4N (γ') phases were found, as reported in previous works using similar nitriding conditions [30]. For the nitrided + DLC specimen, the penetration depth of the X-ray was estimated using the Beer-Lambert equation ($I/I_o = e^{-\mu x}$) [39], where I/I_o is the ratio between absorbed and transmitted beam; x is the penetration depth; μ is the linear absorption coefficient that can be calculated by $\mu_m = \mu/\rho$, ρ is the density; and μ_m is the mass absorption coefficient. For Cu-Kα radiation, λ = 1,5406 Å, the values of μ_m and ρ were obtained from Nist [40]. Assuming an absorption of 64% of the X-ray in the nitride layer, the approximate penetration depth of the X-ray (x) was estimated between 4.51 of 4.66 µm. Therefore, the X-ray was not probing the substrate, justifying the absence of peak 1.

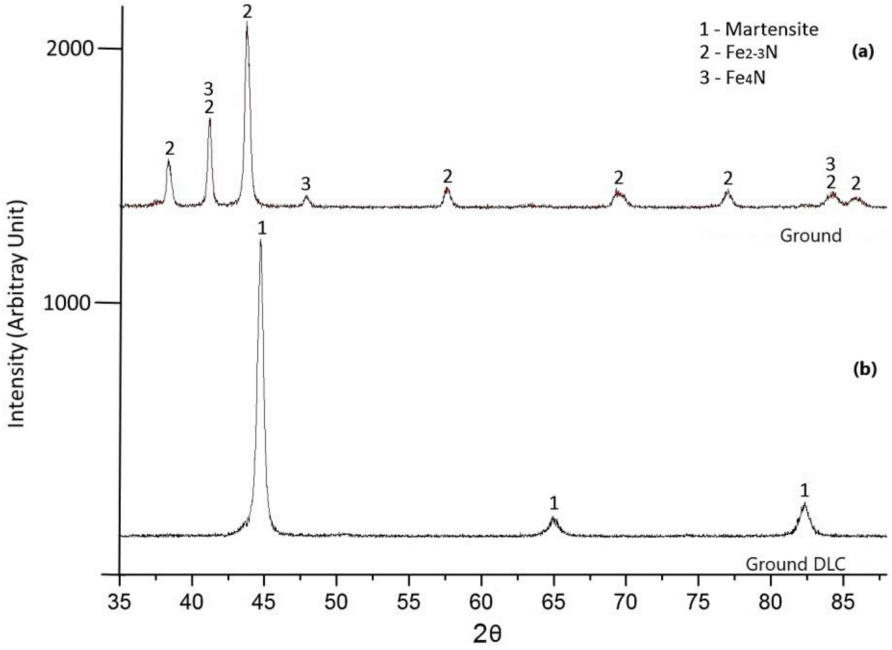

Figure 7. X-ray diffraction (XRD) diffractograms before and after plasma nitriding + DLC: (**a**) ground specimen; (**b**) nitrided specimen + DLC.

The hardness of the different regions (substrate, nitrided layer and DLC coating) were obtained using different methods. The hardness of the substrate and compound layer was measured by Vickers microhardness in polished cross-sections, while the DLC hardness was measured by nanoindentation. Table 4 presents the DLC nanoindentation measurements and calculations for the 14 loading cycles tested; all calculations followed the method proposed by Oliver and Pharr [12], to obtain the Young´s modulus (E) and hardness (H) of the DLC coating. Table 5 summarizes the hardness values for all the regions. Plasma nitriding increased the substrate hardness, with the hardness of the compound layer approximately 65% higher than the substrate. Regarding the hardness of the DLC film, according to the classification given by Hainsworth and Uhure [41], the film can be classified as a-C:H (soft).

Table 4. Results of the nanoindentation tests; E_{red} = Reduced modulus, E = Young´s modulus, H = hardness.

Cycle	E_{red} (GPa)	E (GPa)	H (GPa)
1	43.99	42.42	4.52
2	48.62	47.07	6.71
3	64.07	62.91	7.00
4	37.52	35.96	3.79
5	71.82	71.03	9.58
6	55.06	53.62	5.38
7	63.37	62.19	6.05
8	69.49	68.58	5.47
9	71.67	70.88	6.85
10	52.03	50.53	3.61
11	63.16	61.97	4.85
12	48.31	46.76	4.04
13	72.62	71.88	8.65
14	92.15	92.89	10.08
Average	60.99	59.91	6.18
Standard Deviation	14.41	14.97	2.09

Table 5. Comparison of hardness values for substrate, compound nitrided layer ($HV_{0.1}$) and DLC (nanoindentation).

Region	Hardness (GPa)
Substrate	5.84 ± 0.14
Compound layer	9.61 ± 0.48
DLC	6.18 ± 2.09

Figure 8 presents SEM images of Rockwell C indentations on the ground DLC (Figure 8a,b) and EDT DLC specimens (Figure 8c,d). Radial cracks are observed for both conditions. According to VDI 3198, discussed by Vidakis et al. [42], the presence of radial cracks with little delamination is an indicative of a fragile film with good adhesion. It is also observed the presence of circumferential cracks, evidenced for the ground DLC specimen near the indentation region (Figure 7b). The failures found for both the ground and EDT substrates can be classified as HF3 (acceptable failure), due to the presence of little delamination near the indentation.

Raman spectra for the ground DLC and EDT DLC specimens are presented in Figure 9. As shown in the image, the positions regarding bands D and G are similar for both conditions analyzed. Table 6 summarizes results regarding the position of the peaks D and G, as well as the ratio between the intensity of the peaks D and G (ID/IG) and the amount of hydrogen. Data statistical analysis shows that the results are the same for ground DLC and EDT DLC conditions, indicating that texturing had no influence on the nature of the chemical bonds of the film.

Table 6. Raman analysis results.

Condition	D Peak Position (cm^{-1})	G Peak Position (cm^{-1})	*ID/IG*	%H
VC10 DLC	1394.5 ± 3.5	1588.0 ± 2.0	0.7 ± 0.1	39.0 ± 1.0
EDT DLC	1391.0 ± 1.5	1589.0 ± 1.0	0.7 ± 0.1	39.0 ± 0.0

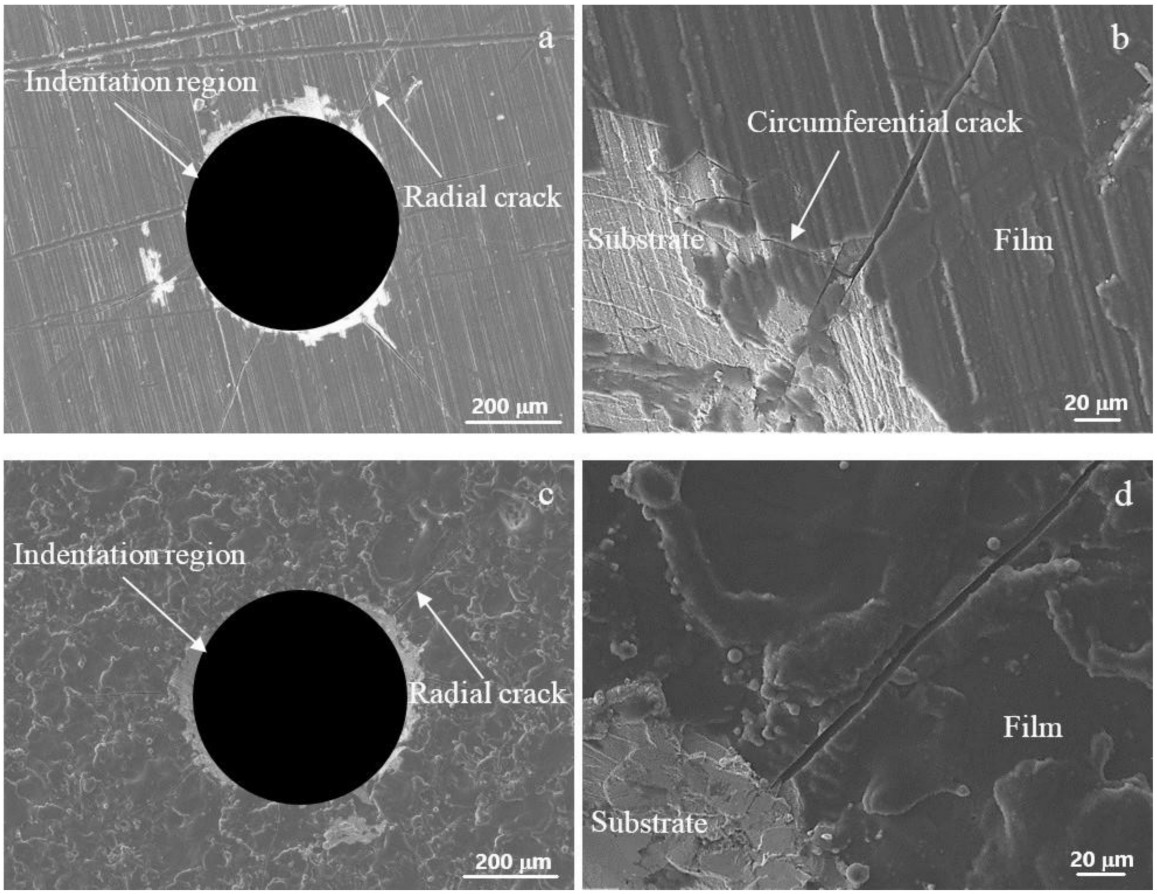

Figure 8. SEM micrographs of the indentations produced by the adhesion test: (**a**,**b**) for the ground DLC specimen; (**c**,**d**) for the EDT DLC specimen. (**a**,**c**) are the indentations and (**b**,**d**) show selected magnified areas in the vicinity of the indentations.

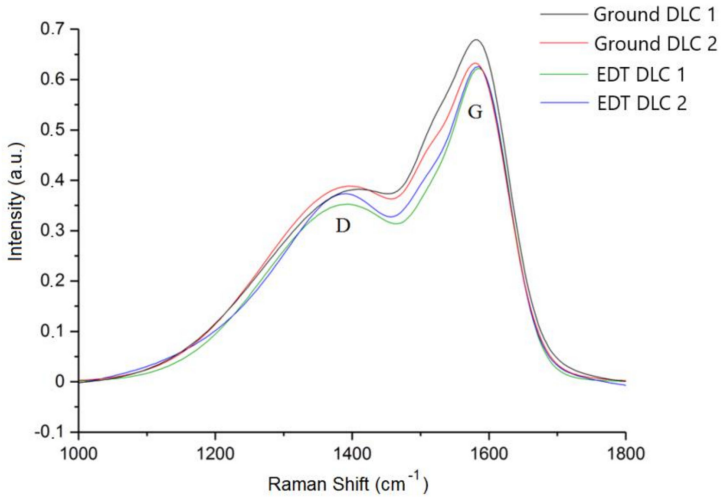

Figure 9. Raman spectra for ground DLC and EDT DLC specimens, two measurements per condition.

XPS analysis was performed for the ground specimen coated with DLC. The atomic composition obtained on the sample surface was 92.9% C and 7.0% O (peaks: C1s 284.0 eV and O1s 531.8 eV). Peak deconvolution for the XPS analysis for C1s was performed using CasaXPS software, shown in Figure 10. Table 7 shows the binding energies of the present species and the corresponding relative percentage. For the equipment used, the error in terms of binding energy was 0.2 eV, in terms of the chemical composition of 5% of the amount of each element.

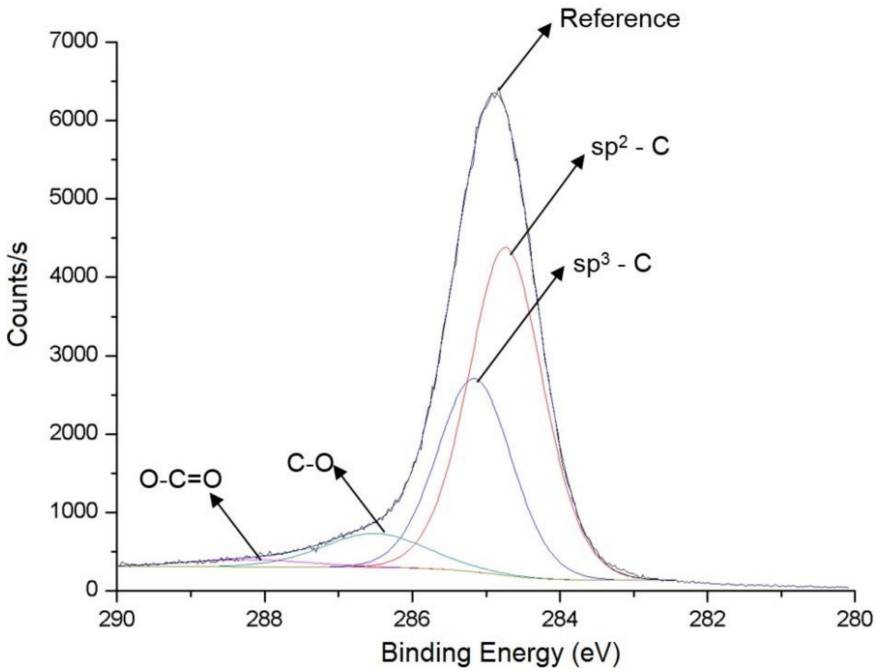

Figure 10. C1s X-ray photoelectron spectroscopy (XPS) spectrum with peak deconvolution for ground DLC specimen.

Table 7. Binding energies of the species and corresponding relative percentages, FWHM = full width at half maximum.

Species	Binding Energy (eV)	FWHM	Relative Percentage (%)
sp^2	284.8	1.2	56.7
sp^3	285.2	1.2	33.2
C-O	286.6	1.6	8.1
O-C=O	288.2	2.0	2.1

3.3. Tribological Performance

Friction coefficient values for the textured specimen and coated specimen under dry and lubricated sliding are presented in Figure 11. For comparative purposes, friction for the ground (non-textured, non-coated) specimen is also presented. Under dry conditions, the EDT specimen presented the highest friction values. In the beginning of the test, friction increased rapidly, achieving almost 0.7, and then reduced to a plateau of around 0.5. Initial friction for the textured specimen coated with DLC was around 0.15, suggesting some lubricity. Friction increased with sliding distance, reaching an approximate plateau of around 0.3. As the sliding distance increased further, friction increased to around 0.38 and then stabilized, but presenting very large scattering. Under lubricated conditions, friction was much more stable and substantially lower. Friction values started at around 0.12, slowly increasing until a value around 0.13 was reached after 100 m of sliding, then remaining fairly constant for the rest of the total sliding distance of 1000 m. When compared with the ground specimen, lubricated friction for the ground specimen was slightly lower, quickly reaching a steady-state value of around 0.10.

Images of the worn tracks are exemplified in Figure 12. Under dry conditions, some damage was observed for the textured specimen coated with DLC after 1000 m of sliding (Figure 12a). The surface damage was confirmed by the 3D topographic maps of the worn tracks (Figure 13a). However, no measurable wear could be accounted for, as confirmed by the selected 2D profile. On the other hand, a large wear scar was formed on the spherical counterbody, which slid against the EDT DLC specimen, as shown in Figure 14a. Under lubricated conditions, the damage was almost imperceptible after 1000 m of sliding

(Figures 12d and 13d), but increased when the sliding distance increased to 1500 m of sliding (Figures 12c and 13c). The ground specimen showed a more distinguishable wear track under lubricated sliding (Figures 12d and 13d); vertical blue lines were used in Figure 12d to emphasize the wear track. The 2D profile showed significant smoothening in the wear track, delimited by the two red vertical lines in Figure 12d. On the other hand, the scar produced on the ball (Figure 14d) was smaller than for the EDT DLC specimen.

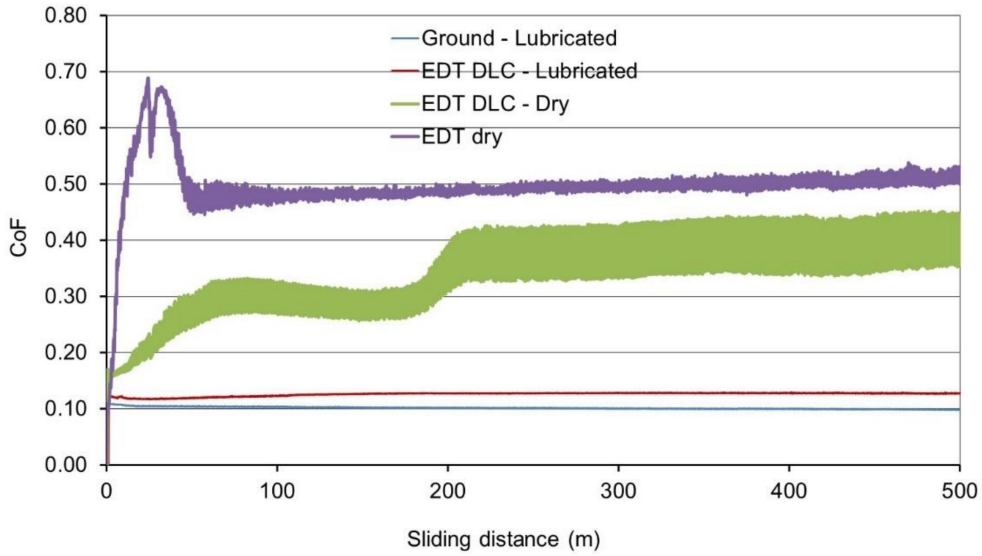

Figure 11. Comparison of the evolution of the coefficient of friction (CoF) with sliding distance.

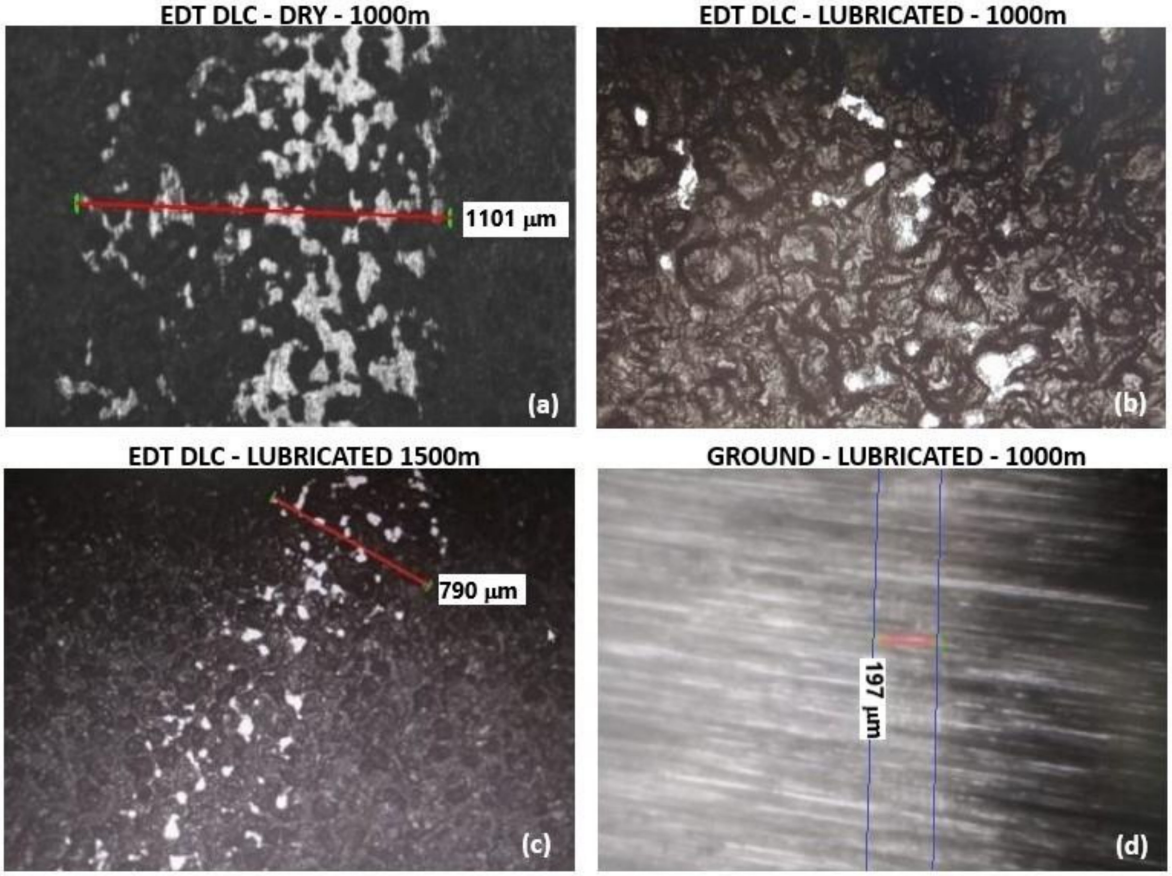

Figure 12. Examples of optical images of the worn tracks under dry and lubricated conditions.

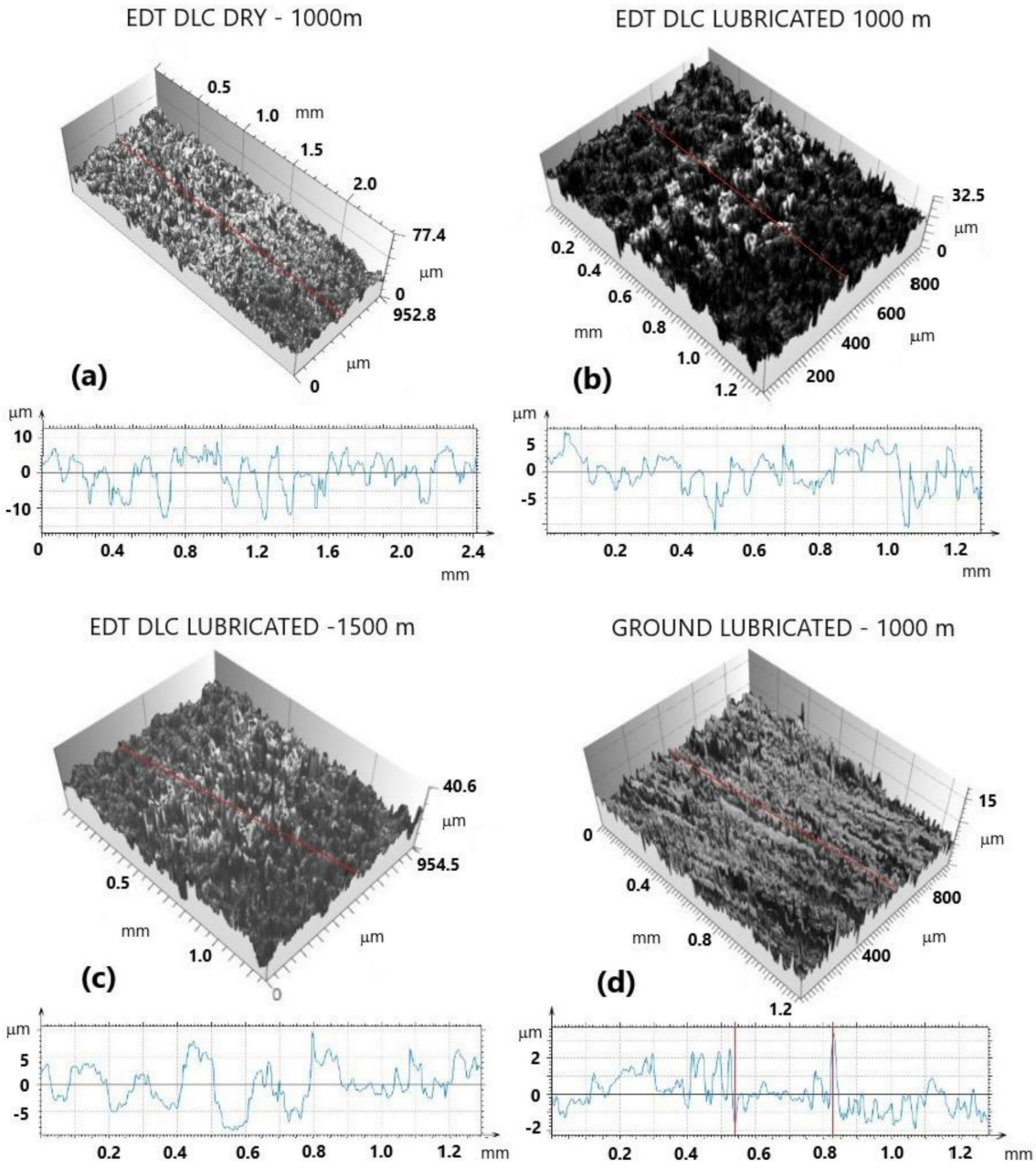

Figure 13. Optical interferometry of the worn tracks (3D maps and selected 2 D profiles: (**a**) EDT DLC dry, 1000 m sliding; (**b**) EDT DLC lubricated, 1000 m sliding; (**c**) EDT DLC lubricated, 1500 m sliding; and (**d**) ground lubricated, 1000 m sliding.

SEM of the worn tracks under higher magnification elucidated better the wear mechanisms for the different specimens. For the textured specimens coated with DLC, the localized damage observed under dry (Figure 15a) and lubricated (Figure 15c) sliding did not seem to result in the complete removal of the DLC film. This was suggested by composition profiles measured by EDX, as exemplified in the EDX composition profile shown in Figure 15e. The clearer regions where damage seemed to occur showed similar chemical composition in relation to the darker regions. For the ground specimen, the worn surface suggested the occurrence of very mild wear, which resulted in substantial smoothening of the surface (Figure 15d).

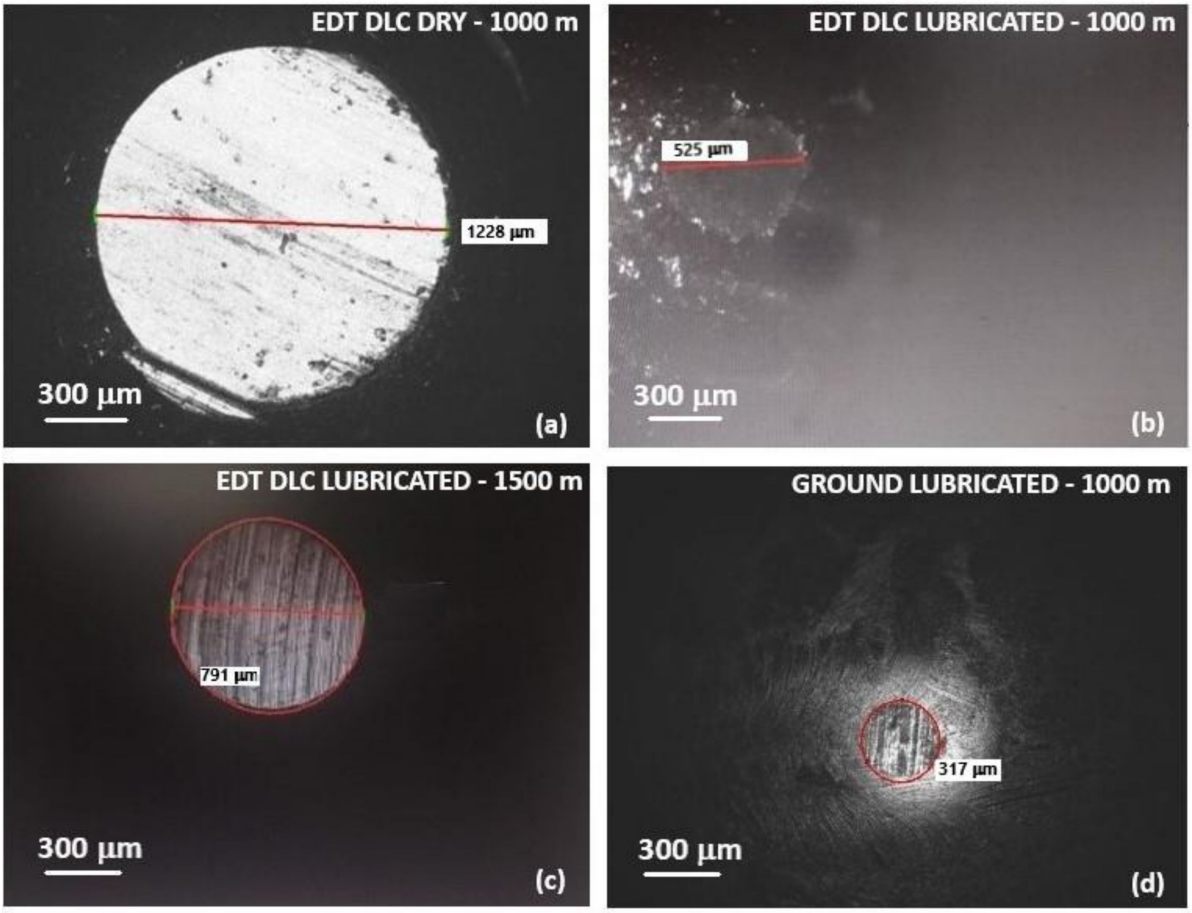

Figure 14. Optical microscopy of the wear scars produced on the balls that slid against the different specimens: (**a**) EDT DLC dry sliding, 1000 m; (**b**) EDT DLC lubricated sliding, 1000 m; (**c**) EDT DLC lubricated sliding, 1500 m; and (**d**) ground-lubricated sliding, 1000 m.

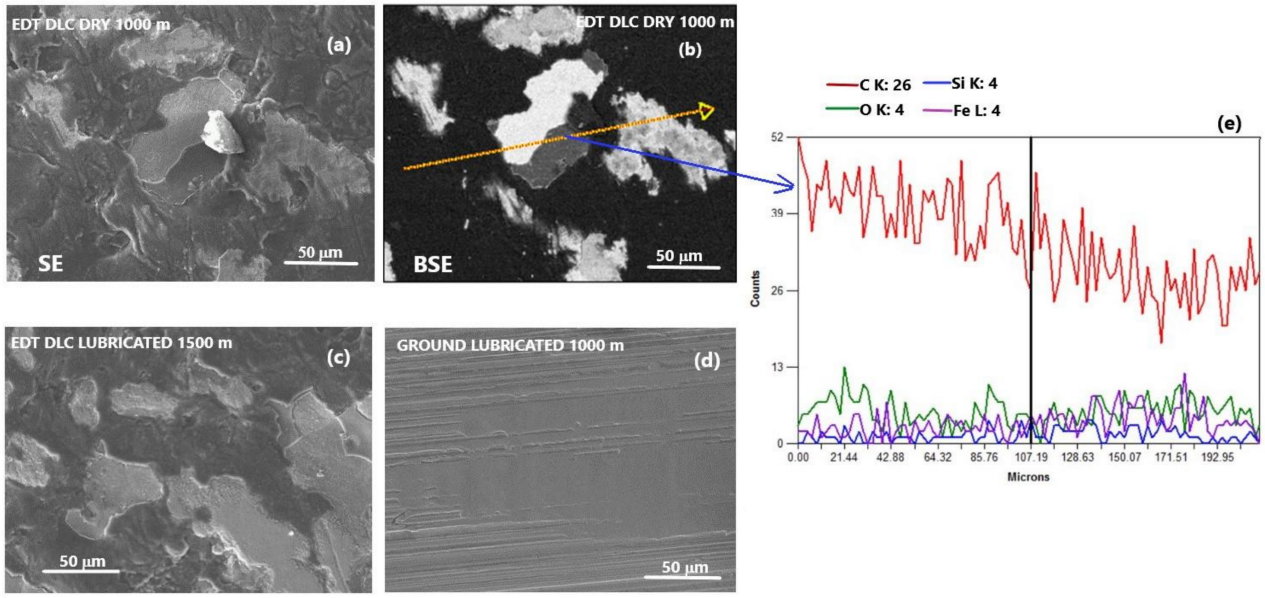

Figure 15. Wear mechanisms observed under SEM: (**a**,**b**) EDT DLC dry, 1000 m sliding, SE image left, BSE image right; (**c**) EDT DLC lubricated, 1500 m sliding; (**d**) ground lubricated, 1000 m sliding; (**e**) EDX composition profile along the line selected in (**b**).

4. Discussion

This work investigated the possibility of using DLC to increase the durability of forming tools previously textured by electrical discharge machining. For that, a multi-layer DLC coating, consisting of a plasma nitrided layer, a Si-rich DLC layer and a top a-C:H layer, was deposited onto tool steel specimens cut from a fragment of a rolling mill roll and then textured by EDT.

Due to high stresses involved in metalforming and the rough nature of the textured specimens, a relatively soft DLC was chosen for this application. It was shown that plasma nitriding before DLC deposition increased the hardness of the substrate to 65%. This increase in hardness improves the film adhesion and/or prevent delamination when applying a transversal load on the sample, as observed in previous works in the literature [43].

Since the roughness of the tool should be transferred to the rolled sheet during the final step of cold rolling, it is very important that the original topography after surface texturing is preserved when DLC is deposited. The results showed that DLC reduced the height and slope of the asperities, and that this reduction was between 2.5 and 4 times higher for the textured specimens than for the ground specimens. Moreover, the *Sku* versus *Ssk* morphological space showed very significant changes when DLC was deposited for the textured tools, but not for the ground tools. The EDT tools lied in the upper left quadrant, and presented very large scattering. This probably occurred as a result of the nature of the EDT process, achieved using the principles of electrical discharge machining. The ablation mechanism in electrical discharge machining leads to the formation of craters, but rapid cooling due to the contact with the cold dielectric fluid leads to resolidification, producing some protruding features [44]. The machining parameters were chosen to mainly produce large craters, therefore *Ssk* of surfaces textured by EDT should be mostly very negative due to the presence of the craters, yet measurements in the few regions with protruding resolidified material should account for the large scattering observed in the *Ssk* values. Similar explanation is valid for the large values of *Sku* and the large scattering of the results. Some measured regions probably presented irregularities with very similar heights, giving very high *Sku* values, whereas other regions presented both craters and resolidified features, giving a more Gaussian height distribution and then lower *Sku* values. When the textured tool was coated with DLC, the smoothening effect conferred by the coating drastically reduced the scattering of the *Ssk* and *Sku* values. Moreover, the height distribution became much more Gaussian and then *Sku* approached 3. The average value of *Ssk* value increased with DLC coating, yet it remained negative, evidencing a preponderance of valleys.

The change in surface topography parameters is a limitation for the use of DLC in textured tools, and needs to be taken into account when designing the texturing step of the tools. For instance, EDT could be set up to produce rougher surfaces, so that after DLC deposition, the final roughness lied within the desired range for the tool. One important positive aspect is that DLC increased the load bearing capacity of the textured tools (see *Sbi* values in Figure 6).

In terms of the adhesion of the DLC film, both the ground and the textured substrates resulted in coatings that were classified as HF3 (acceptable failure). Moreover, circumferential cracks were observed for the ground substrate (Figure 8b) near the indentation region due to the action of tensile stresses in the region caused by the pile-up of the substrate (deformation), as discussed by Souza et al. [45], and more recently confirmed by Gilewicz et al. [46].

The Raman results allowed to characterize the structure of the DLC. The *ID*/*IG* ratio is a way of monitoring the carbon bonds present in the film; in amorphous carbon *ID*/*IG* represents a measure of the size of the sp^2 phase organized in rings [36]. According to Al Mahmud et al. [47], the higher the *ID*/*IG* ratio the greater the number of sp^2 bonds in the ring structure of the film, indicating a reduction in the amount of sp^3 bonds. Soprano et al. obtained *ID*/*IG* variations from 0.64 to 0.72 with different samples' texturing conditions produced via sanding processes, and indicated that these variations were not significant [29]. The bands' positions (D and G), *ID*/*IG* ratio and the percentage of hy-

drogen in the present work were similar to the values in Soprano´s work. XPS analysis complemented the characterization of the DLC films. To perform the deconvolution of C1s peak, peaks similar to those found in the work of Al Mahmud et al. [47] were observed. The contamination represented by the C-O and O-C + O bonds is observed because the analysis was carried out on the sample surface, indicating that there was a reaction of the film with atmospheric oxygen. Considering the deconvolution of C1s peak, the alternative would be the adjustment with four sub-peaks: 284.4 eV, 285.1 eV, 286.5 eV, 288.4 eV, related to groups CC sp^2, CC sp^3, CO and OC=O, respectively, with the proportion of CC sp^2/CC sp^3 sub-peaks equal to 56.68/33.17. However, this determination of the proportion between C-C sp^2 and C-C sp^3 is questioned in the literature, as the separation in binding energy between the components is very small, which leaves much freedom in the mathematical adjustment, with Gaussians, for example (experimental analysis). Therefore, a possibility published by Turgeon and Paynter is to use the Auger carbon spectra (as a function of kinetic energy) to determine the separation (D) between the maximum and the minimum [48]. The result indicates a proportion of 40% C-C sp^3. The combination of the Raman analysis, XPS analysis and nanoindentation measurements confirmed that the DLC film was relatively soft and consisted of a -C:H.

Under dry sliding, the textured specimen showed very high initial friction values, reaching almost 0.7, and then stabilized at 0.5. These values are in the same range of friction values measured in [8] for EDT specimens of similar material, although the test configuration was very different (dry reciprocating sliding, line contact). In that same work [8], the friction values for specimens textured by EDT and for EDT + plasma nitriding were similar. In the present work, when the EDT specimens were plasma-nitrided and then coated with DLC, an initial coefficient of friction of around 0.15 was measured, consistent with the solid lubricating nature of the film. However, as the sliding distance increased, friction increased first to an initial plateau of 0.3, and then a second plateau of around 0.4. This should be related to the very rough nature of the substrate, which should increase the deformation component of friction. However, the values were substantially lower than those measured for similar textured specimens coated with hard chrome under dry reciprocating sliding and high-contact pressure conditions [5,8]. Moreover, even in the final plateau region of the friction curve, there should be some contribution of the solid lubricant nature of the DLC film, since the worn surfaces after 1000 m of sliding showed that the damaged regions in the wear tracks were rich in C and Si. It is plausible that the top DLC layer was removed, but the intermediate Si-rich DLC layer remained even after long sliding distances under dry conditions. Under lubricated conditions, friction was substantially lower and much more stable, with values typical of boundary lubrication. The Dowson and Hamrock equation for an EHL elliptical contact [49] (Equation (3)) was used to estimate the film thickness in the central region of the contact (h_c) during the tests

$$\frac{h_{min}}{R'_x} = 2.69U'^{0.67}G^{0.53}W'^{-0.067}\left(1 - 0.61e^{-0.73\left(\frac{R'_y}{R'_x}\right)^{0.73}}\right) \quad (3)$$

$$U' = \frac{U\eta}{ER'_x} \quad (4)$$

$$\frac{1}{E*} = \frac{1-v_1^2}{E_1} + \frac{1-v_2^2}{E_2} \quad (5)$$

$$G = \alpha E^* \quad (6)$$

$$W' = \frac{W}{ER'^2_x} \quad (7)$$

where $R_x = R_y$ = ball radius (3 mm); E^* is the combined Young´s modulus of the two contacting materials given by $1/E^* = (1 - {\nu_1}^2)/E_1 + (1 - {\nu_2}^2)/E_2$, U is the sliding speed (0.3 m·s^{-1}), W is the normal load (10 N), η is the lubricant dynamic viscosity (38.55 mPa.s) and α is the lubricant piezoviscous coefficient, estimated as 21.3 GPa^{-1} using the empirical

equation $\alpha \approx (0.6 + 0.965 \log(\eta)\, 10^{-8})$. This gave values of h_{min} = 252 nm and h_{min} = 229 nm for the coated and uncoated specimens, respectively. These values are lower than the roughness of the specimens (including for the ground specimen), confirming that the tests run under boundary lubrication conditions. The higher friction values for the EDT DLC specimen, when compared with the uncoated ground specimen, should be related to its larger roughness, increasing the deformation component of friction.

Wear of the textured specimen when coated with DLC under dry sliding was not measurable, although some surface damage was visible after 1000 m of sliding. Since the coating should protect the topography of the textured roll against wear, the change in surface topography after the sliding tests is very relevant to assess the adequacy of the coating. Comparing surface topography measurements inside the worn tracks with the original parameters for the textured specimen coated with DLC, after the sliding tests *Sq*, *Spk* and *Svk* reduced to 4.7%, 3.0% and 12.8%, respectively, whereas *Sdq* increased to 17.5%. Such variations can be considered small for dry tests under high contact pressures. Under real rolling conditions, the changes of topographic parameters for a textured roll coated with hard chrome between the new condition and after a rolling campaign were around a 50% reduction of *Sq*, 50% reduction of *Sdq* and 60% reduction of *Spk* [50]. Under lubricated conditions, the changes in topographic parameters (not presented) were not statistically significant.

Despite the relatively low hardness, the soft DLC resulted in small spallation on a rough surface, and could withstand high contact pressures with adequate tribological performance, paving a possible way for its future use in textured metalforming tools. The results showed that the occurrence of spallation was very small, and the tribological performance was at least comparable (or superior) to results in the literature regarding friction and wear of textured tool materials coated with hard chrome using ball-on-flat tests [8,50].

Another important contribution of this work relates to the quantification of changes caused by DLC deposition on surface topography. Although plasma nitriding is known to increase surface roughness [27,34], the combined used of plasma nitriding and DLC coatings produced smoother surfaces. This should be true not only for EDT surfaces, but for very rough substrates in general. From the point of view of a textured roll, this is a negative aspect, as the roughness of the roll needs to be imprinted onto the rolled sheet. On the other hand, for other applications, the combined use of plasma nitriding and DLC coating on a very rough substrate could result in surfaces with a superior load bearing capacity.

5. Conclusions

This work investigated the deposition of a multilayer DLC coating onto textured tool steel specimens, aiming to assess its suitability to increase the durability of textured rolls in cold rolling operations. The results showed that:

1. The coating was classified as a soft multilayer coating consisting of a plasma nitride layer for load support, a Si-rich interlayer to improve adhesion and an a-C:H top layer.
2. The deposition of DLC significantly reduced the roughness of the textured specimens. This needs to be accounted for when designing the textures of the rolls.
3. DLC protected the textured surfaces under dry sliding, providing stable and relatively low friction and negligible wear even after 1000 m of sliding.
4. The changes in surface topography due to dry sliding of the textured and coated surfaces were considered small. Changes in surface topography under lubricated sliding were not statistically significant for any of the specimens.

Author Contributions: Conceptualization, H.L.C., J.C.G.M. and J.D.B.d.M.; methodology, E.A.d.S.d.A., H.L.C., J.C.G.M. and J.D.B.d.M.; specimen production, C.B.; investigation, E.A.d.S.d.A., C.E.d.C. and J.C.G.M.; resources, J.C.G.M., C.E.d.C. and C.B.; writing—original draft preparation, E.A.d.S.d.A. and H.L.C.; writing—review and editing, J.D.B.d.M. All authors have read and agreed to the published version of the manuscript.

Funding: E.A. received funding from Coordenação de Aperfeiçoamento de Pessoal de Nível Superior (CAPES, Brazil)—Finance Code 001; H.L.C. acknowledges financial support from Conselho Nacional de Desenvolvimento Científico e Tecnológico (CNPq, Brazil), grant number 305453/2017-3.

Institutional Review Board Statement: Not applicable.

Informed Consent Statement: Not applicable.

Data Availability Statement: Data is contained within the article.

Acknowledgments: Gerdau S.A. provided the roll fragments to produce the tool steel specimens.

Conflicts of Interest: The authors declare no conflict of interest.

References

1. Aizawa, T.; Wasa, K.; Tamagaki, H. A DLC-Punch Array to Fabricate the Micro-Textured Aluminum Sheet for Boiling Heat Transfer Control. *Micromachines* **2018**, *9*, 147. [CrossRef]
2. Flegler, F.; Neuhäuser, S.; Groche, P. Influence of sheet metal texture on the adhesive wear and friction behaviour of EN AW-5083 aluminum under dry and starved lubrication. *Tribol. Int.* **2020**, *141*, 105956. [CrossRef]
3. Hetzner, H.; Koch, J.; Tremmel, S.; Wartzack, S.; Merklein, M. Improved Sheet Bulk Metal Forming Processes by Local Adjustment of Tribological Properties. *J. Manuf. Sci. Eng. Trans. Asme* **2011**, *133*. [CrossRef]
4. Costa, H.L.; Hutchings, I.M. Effects of die surface patterning on lubrication in strip drawing. *J. Mater. Process. Technol.* **2009**, *209*, 1175–1180. [CrossRef]
5. De Mello, J.D.B.; Gonçalves, J.L., Jr.; Costa, H.L. Influence of surface texturing and hard chromium coating on the wear of steels used in cold rolling mill rolls. *Wear* **2013**, *302*, 1295–1309. [CrossRef]
6. Tillmann, W.; Grisales, D.; Stangier, D.; Butzke, T. Tribomechanical Behaviour of TiAlN and CrAlN Coatings Deposited onto AISI H11 with Different Pre-Treatments. *Coatings* **2019**, *9*, 519. [CrossRef]
7. Elmkhah, H.; Mahboubi, F.; Abdollah-Zadeh, A.; Rouhaghdam, A.R.S. A new approach to improve the surface properties of H13 steel for metal forming applications by applying the TiAlN multi-layer coating. *J. Manuf. Process.* **2018**, *32*, 873–877. [CrossRef]
8. Gonçalves, J.L.; De Mello, J.D.B.; Costa, H.L. Tribological behaviour of alternative surface modifications for cold rolling mill rolls. *Wear* **2021**, *470–471*, 203614. [CrossRef]
9. Tavares, A.F.; Lopes, A.P.O.; Mesquita, E.A.; Almeida, D.T.; Souza, J.H.C.; Costa, H.L. Friction and wear mechanisms in coated forming tools. *Wear* **2020**. accepted for publication.
10. Jean, M.D.; Lian, G.F.; Chen, B.S. Tribological Behaviors of DLC Films and their Application in Micro-Deep Drawability. *Acta Phys. Polon. A* **2018**, *134*, 429–433. [CrossRef]
11. Podgornik, B.; Jerina, J. Surface topography effect on galling resistance of coated and uncoated tool steel. *Surf. Coat. Technol.* **2012**, *206*, 2792–2800. [CrossRef]
12. Elkoca, O. A study on the characteristics of electrical discharge textured skin pass mill work roll. *Surf. Coat. Technol.* **2008**, *202*, 2765–2774. [CrossRef]
13. Pawelski, I.O.; Rasp, I.W.; Zwick, W.; Nettelbeck, I.H.J.; Steinhoff, I.K. The influence of different work-roll texturing systems on the development of surface structure in the temper rolling process of steel sheet used in the automotive industry. *J. Mater. Process. Technol.* **1994**, *45*, 215–222. [CrossRef]
14. Bech, J.; Bay, N.; Eriksen, M. A Study of Mechanisms of Liquid Lubrication in Metal Forming. *CIRP Ann. Manuf. Technol.* **1998**, *47*, 221–226. [CrossRef]
15. Simao, J.; Aspinwall, D.K. Hard chromium plating of EDT mill work rolls. *J. Mater. Process. Technol.* **1999**, *93*, 281–287. [CrossRef]
16. Brooman, E.W. Wear behavior of environmentally acceptable alternatives to chromium coatings: Cobalt-based and other coatings. *Metal Finish.* **2004**, *102*, 42–54. [CrossRef]
17. Lausmann, G.A. Electrolytically deposited hardchrome. *Surf. Coat. Technol.* **1996**, *86–87*, 814–820. [CrossRef]
18. Chiu, L.H.; Yang, C.F.; Hsieh, W.C.; Cheng, A.S. Effect of contact pressure on wear resistance of AISI H13 tool steels with chromium nitride and hard chromium coatings. *Surf. Coat. Technol.* **2002**, *154*, 282–288. [CrossRef]
19. Ma, C.; Wang, S.C.; Wang, L.P.; Walsh, F.C.; Wood, R.J.K. The electrodeposition and characterisation of low-friction and wear-resistant Co-Ni-P coatings. *Surf. Coat. Technol.* **2013**, *235*, 495–505. [CrossRef]
20. Aisenberg, S.; Chabot, R. Ion-beam deposition of thin films of diamondlike carbon. *J. Appl. Phys.* **1971**, *42*, 2953–2958. [CrossRef]
21. Robertson, J. Amorphous carbon thin films. *Mater. Sci. Eng. R* **2002**, *37*, 129–281. [CrossRef]
22. Bonelli, M.; Miotello, A.; Ossi, P.M.; Pessi, A.; Gialanella, S. Laser-irradiation-induced structural changes on graphite. *Phys. Rev. B* **1999**, *59*, 13513–13516. [CrossRef]
23. Shum, P.W.; Zhou, Z.F.; Li, K.Y. To increase the hydrophobicity, non-stickiness and wear resistance of DLC surface by surface texturing using a laser ablation process. *Tribol. Int.* **2014**, *78*, 1–6. [CrossRef]
24. Michalek, A.; Qi, S.J.; Batal, A.; Penchev, P.; Dong, H.S.; See, T.L.; Dimov, S. Sub-micron structuring/texturing of diamond-like carbon-coated replication masters with a femtosecond laser. *Appl. Phys. A Mater. Sci. Process.* **2020**, *126*, s00339–s020. [CrossRef]

25. Corbella, C.; Portal-Marco, S.; Rubio-Roy, M.; Bertran, E.; Oncins, G.; Vallve, M.A.; Ignes-Mullol, J.; Andujar, J.L. Modifying surface properties of diamond-like carbon films via nanotexturing. *J. Phys. D Appl. Phys.* **2011**, *44*. [CrossRef]
26. Erdemir, A.; Eryilmaz, O. Achieving superlubricity in DLC films by controlling bulk, surface, and tribochemistry. *Friction* **2014**, *2*, 140–155. [CrossRef]
27. De Mello, J.D.B. Carbon Based Coatings for Hermetic Compressor Applications. *Adv. Sci. Technol.* **2014**, *89*, 21–30. [CrossRef]
28. Lara, L.C.; Costa, H.L.; de Mello, J.D.B. Influence of layer thickness on sliding wear of multifunctional tribological coatings. *Ind. Lubr. Tribol.* **2015**, *67*, 460–467. [CrossRef]
29. Soprano, P.B.; Salvaro, D.B.; Giacomelli, R.O.; Binder, C.; Klein, A.N.; de Mello, J.D.B. Effect of soft substrate topography on tribological behavior of multifunctional DLC coatings. *J. Braz. Soc. Mech. Sci. Eng.* **2018**, *40*, 371. [CrossRef]
30. Shioga, P.H.T.; Binder, C.; Hammes, G.; Klein, A.N.; Mello, J.D.B.d. Effects of different plasma nitrided layers on the tribological performance of DLC coatings. *Mater. Res.* **2016**, *19*, 1180–1188. [CrossRef]
31. Holmberg, K.; Laukkanen, A.; Ronkainen, H.; Waudby, R.; Stachowiak, G.; Wolski, M.; Podsiadlo, P.; Gee, M.; Nunn, J.; Gachot, C.; et al. Topographical orientation effects on friction and wear in sliding DLC and steel contacts, part 1: Experimental. *Wear* **2015**, *330–331*, 3–22. [CrossRef]
32. Binder, C.; Bendo, T.; Hammes, G.; Klein, A.; de Mello, J. Effect of nature of nitride phases on sliding wear of plasma nitrided sintered iron. *Wear* **2015**, *332*, 995–1005. [CrossRef]
33. Jack, K. The synthesis and characterization of bulk α ″-Fe16N2. *J. Alloy. Compd.* **1995**, *222*, 160–166. [CrossRef]
34. Kovacı, H.; Yetim, A.F.; Baran, Ö.; Çelik, A. Tribological behavior of DLC films and duplex ceramic coatings under different sliding conditions. *Ceram. Int.* **2018**, *44*, 7151–7158. [CrossRef]
35. Rosenkranz, A.; Costa, H.L.; Baykara, M.Z.; Martini, A. Synergetic Effects of Surface Texturing and Solid Lubricants to Tailor Friction and Wear—A Review. *Wear* **2021**. [CrossRef]
36. Casiraghi, C.F.A.R.J.; Ferrari, A.C.; Robertson, J. Raman spectroscopy of hydrogenated amorphous carbons. *Phys. Rev. B* **2005**, *72*, 085401. [CrossRef]
37. Cho, S.-J.; Lee, K.-R.; Yong Eun, K.; Hee Hahn, J.; Ko, D.-H. Determination of elastic modulus and Poisson's ratio of diamond-like carbon films. *Thin Solid Films* **1999**, *341*, 207–210. [CrossRef]
38. De Mello, J.D.B.; Durand-Charre, M.; Mathia, T. Abrasion mechanisms of white cast iron I: Influence of the metallurgical structure of molybdenum white cast irons. *Mater. Sci. Eng.* **1985**, *73*, 203–213. [CrossRef]
39. Cullity, B.D.; Stock, S.R. *Elements of X-ray Diffraction*, 3rd ed.; Prentice-Hall: New York, NY, USA, 2014. [CrossRef]
40. NIST. X-Ray Mass Attenuation Coefficients. Available online: https://www.nist.gov/pml/x-ray-mass-attenuation-coefficients (accessed on 1 February 2021).
41. Hainsworth, S.V.; Uhure, N. Diamond like carbon coatings for tribology: Production techniques, characterisation methods and applications. *Int. Mater. Rev.* **2007**, *52*, 153–174. [CrossRef]
42. Vidakis, N.; Antoniadis, A.; Bilalis, N. The VDI 3198 indentation test evaluation of a reliable qualitative control for layered compounds. *J. Mater. Process. Technol.* **2003**, *143*, 481–485. [CrossRef]
43. Komarov, F.; Konstantinov, V.; Kovalchuk, A.; Konstantinov, S.; Tkachenko, H. The effect of steel substrate pre-hardening on structural, mechanical, and tribological properties of magnetron sputtered TiN and TiAlN coatings. *Wear* **2016**, *352*, 92–101. [CrossRef]
44. Arantes, L.J.; da Silva, E.R.; dos Santos, R.F.; Sales, W.F.; Raslan, A.A. The electrical discharge machining process aided by abrasive jet. *Int. J. Adv. Manuf. Technol.* **2016**, *87*, 411–420. [CrossRef]
45. Souza, R.; Sinatora, A.; Mustoe, G.; Moore, J. Numerical and experimental study of the circular cracks observed at the contact edges of the indentations of coated systems with soft substrates. *Wear* **2001**, *251*, 1337–1346. [CrossRef]
46. Gilewicz, A.; Jedrzejewski, R.; Myslinski, P.; Warcholinski, B. Structure, Morphology, and Mechanical Properties of AlCrN Coatings Deposited by Cathodic Arc Evaporation. *J. Mater. Eng. Perform.* **2019**, *28*, 1522–1531. [CrossRef]
47. Al Mahmud, K.; Varman, M.; Kalam, M.; Masjuki, H.H.; Mobarak, H.; Zulkifli, N. Tribological characteristics of amorphous hydrogenated (aC: H) and tetrahedral (ta-C) diamond-like carbon coating at different test temperatures in the presence of commercial lubricating oil. *Surf. Coat. Technol.* **2014**, *245*, 133–147. [CrossRef]
48. Turgeon, S.; Paynter, R. On the determination of carbon sp^2/sp^3 ratios in polystyrene–polyethylene copolymers by photoelectron spectroscopy. *Thin Solid Films* **2001**, *394*, 43–47. [CrossRef]
49. Hamrock, B.T.; Dowson, D. *Ball Bearing Lubrication: The Elastohydrodynamics of Elliptical Contacts*; Wiley: New York, NY, USA, 1981. [CrossRef]
50. Gonçalves, J.L., Jr.; De Mello, J.D.B.; Costa, H.L. Wear in cold rolling milling rolls: A methodological approach. *Wear* **2019**, *426–427 Pt B*, 1523–1535. [CrossRef]